encit 2020

ABCM

18th Brazilian Congress of Thermal Sciences and Engineering
November 16-20, 2020 (Online)

ENC-2020-0303
NUMERICAL VALIDATION OF A MICRO PELTON TURBINE FOR DIFFERENT OPERATIONAL CONDITIONS

Rafael Cordebela Salgado
Washington Orlando Irrazabal Bohorquez
Federal University of Juiz de Fora, Rua José Lourenço Kelmer, Campus Universitário, CEP: 36036-900 - Juiz de Fora – MG, Brazil
rafael.salgado@engenharia.ufjf.br, wirraz@engenharia.ufjf.br

Júlio César Costa Campos
Federal University of Viçosa, Av. Peter Henry Rolfs, Campus Universitário, CEP: 36570-900, Viçosa – MG , Brazil
julio.campos@ufv.br

Abstract. *The aim of this paper was to compare Computational Fluid Dynamics and experimental results for the torque as a function of the rotation speed for a Pelton turbine scaled model. Multiphase flow simulations of free surface, testing the mesh dependence and different operational points in the design condition of the turbine were implemented. The simulations were conducted to validate the torque measurement calculated by the Computational Fluid Dynamics model, doing as much simplifications as possible, due to the axial symmetry of the turbine, to reduce computational costs. Succinct comments regarding the flow in the buckets are also shown in this work. Results discrepancies ranged from 4 to 8% and are larger for higher rotation speeds.*

Keywords: *Pelton turbine, Computational Fluid Dynamics, multiphase flow, torque*

1. INTRODUCTION

Pelton turbines are hydraulic impulse turbomachinery, which means that the available energy from water is converted into kinetic energy. The multiphase flow of free surface between water and air due to the interaction of the jet with the buckets and the outlet of the turbine into the atmosphere makes the simulation complex, in addition to the constructive shape of the buckets. Computational Fluid Dynamics (CFD) solve flows problems through the implementation of numerical methods.

Some researches about the total torque generated in Pelton turbines are shown in the literature. (Gupta et al., 2016) designed 10 buckets and 3 jets, totaling a computational grid with approximately 7 million cells, which in terms of computational cost lasted for about 75 hours. (Barstad, 2012; Nigussie et al., 2017; Panthee et al., 2014 and Rygg, 2013) used only 3 consecutive buckets, upon which the torque was measured only in the middle bucket. With the torque of the middle bucket, it was then possible to build the torque of the entire rotor, assuming that each bucket would have the same loading. In this approach, the torque of the middle bucket is influenced by the water flow generated by the first bucket, which reaches the middle bucket at the rear, and by the third bucket, so the jet is cut when it impacts the middle bucket. The simulation with only 3 buckets allows better local control of the mesh and therefore, better precision of the results, as described in (Nigussie et al., 2017).

A detailed review of the literature about simulations in Pelton turbines was carried out by (Židonis and Aggidis, 2015). In that review, literatures that used simulations by the Fast Lagrangian Simulation (FLS) method, OpenFOAM and Ansys products (CFX and Fluent) were approached. The conclusion of that review shows that, nowadays, the Ansys-CFX code is the most used and indicated in terms of multiphase simulations in Pelton turbines.

This work is based on numerical modeling and experimental data of a micro Pelton turbine from the Laboratory of Thermal and Hydraulic Sciences in the Department of Mechanical and Industrial Engineering at the Federal University of Juiz de Fora, designed for didactic purposes by the manufacturer Tecquipment. The turbine does not follow the main design recommendations suggested by (Eisenring, 1991) and (Thake, 2000) in which the main measurements of the turbine are related to the jet diameter. The manufacturer provides a data acquisition system called VDAS, which was used to record experimental data.

Experimental results are very important to validate a Computational Fluid Dynamics model. The bucket geometry of the Pelton Wheel was used to define the fluid domain and meshing that domain. These numerical and experimental results

are compared. The numerical results calculated for the torque overestimate the experimental outcomes up to 8.5%, approximately. Additionally, this work shows a brief discussion of the flow behavior through the turbine buckets.

This manuscript presents an entire methodology for multiphase modeling in Pelton turbines and its validation. From the validation of a CFD model, it is possible to use the same model for numerical simulations in other Pelton turbines and to perform geometric optimizations in the turbine, in order to improve its efficiency.

2. METHODOLOGY

2.1 CAD modeling and computational domain

Several measurements were made on the buckets, checking the output angle of 165° and the splitter angle of 18°. Exploring the axial symmetry of the turbine and in order to reduce computational costs, only three half buckets and half jet were modeled. The bucket design consists of the construction of several cross sections, each one keeping the output angle and the splitter angle. This is shown in Fig. 1.

After modeling a single bucket, two distinct domains were elaborated: stationary and rotating, as seen in Fig. 2 and 3, respectively.

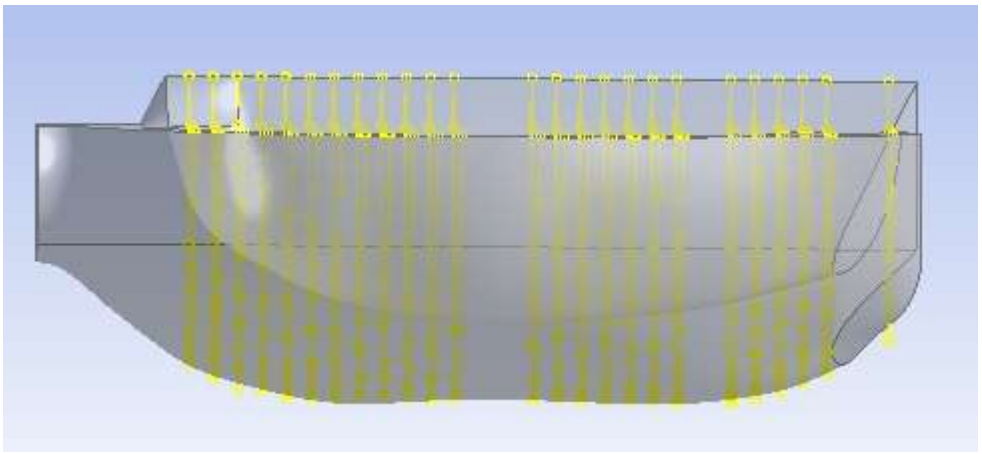

Figure 1: Bucket design.

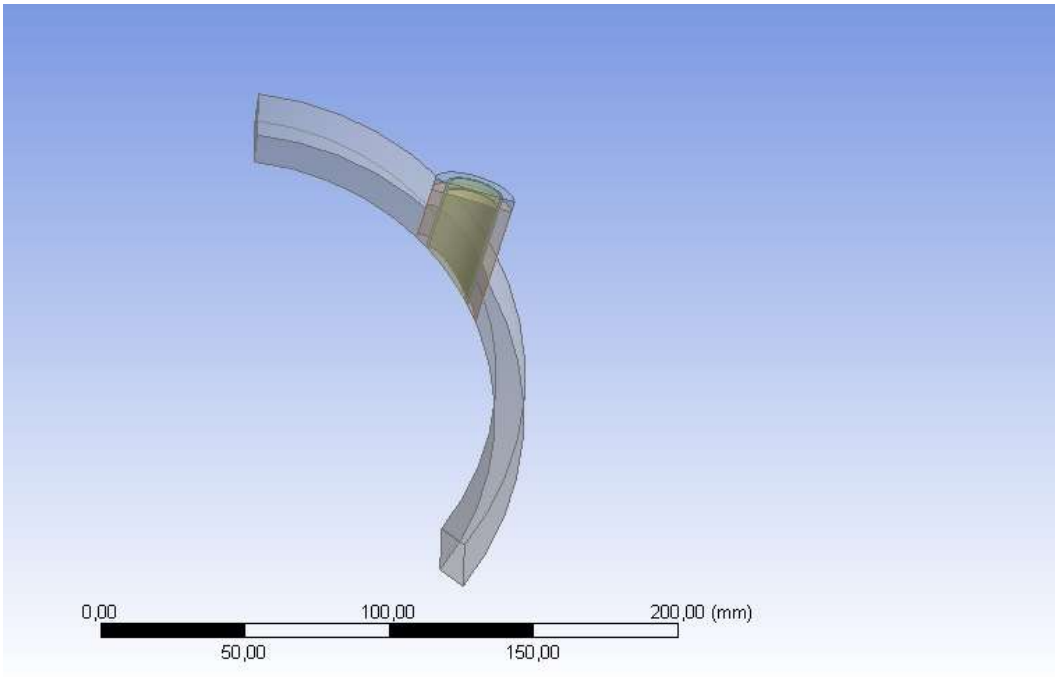

Figure 2: Stationary domain.

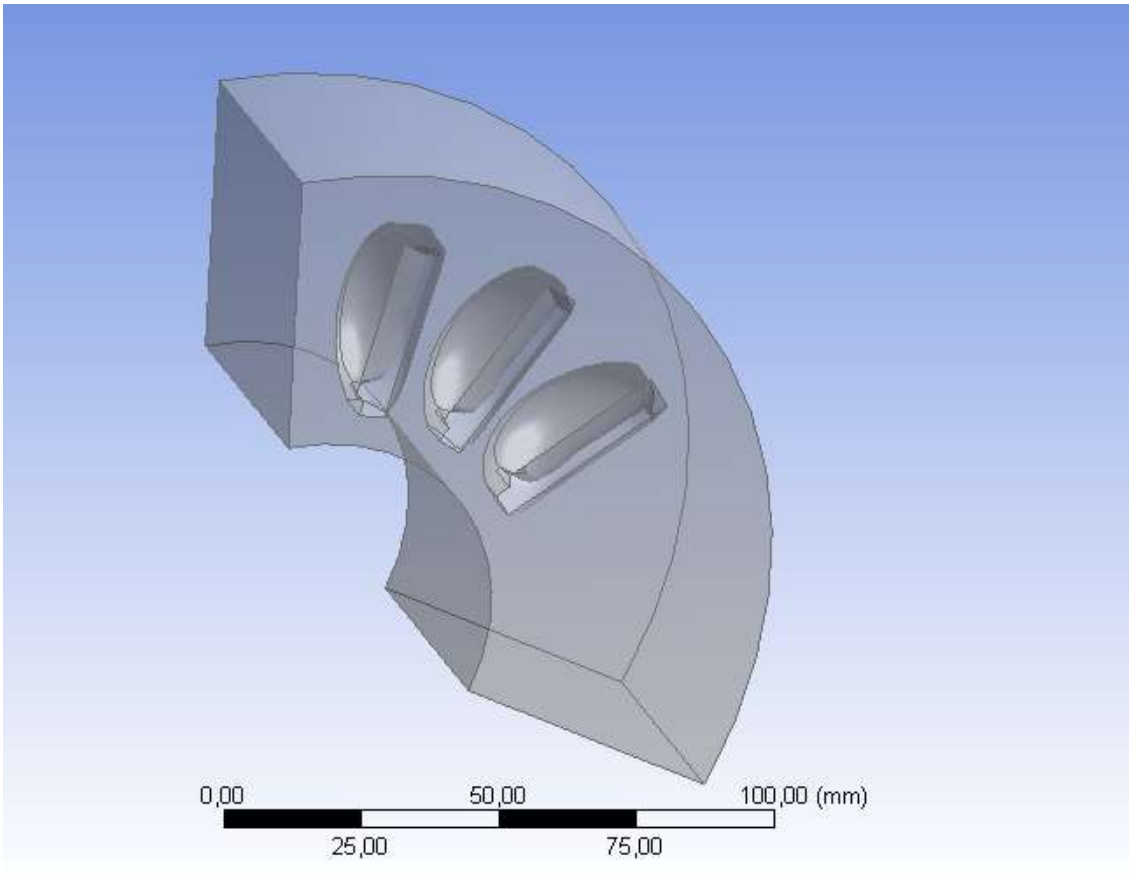

Figure 3: Rotating domain.

2.2 Turbulence modeling

After a discretization of the computational mesh, the homogeneous multiphase model of free surface was chosen.

Water Volume Fractions were initially defined for each domain, this value varies between 0 and 1. A surface tension model with a water-air surface tension coefficient of 0.0728 N/m (White, 2011) was also defined. The timesteps, which correspond to the interval in which the solver calculates the results have been set to 0.0002s. Transient scheme was the Second Order Backward Euler. The residual target was chosen as 10^{-4}, for conservation equations.

Symmetry conditions were imposed, and an expression was defined to calculate the total simulation time. Such expression corresponds to the time that the rotor takes to perform a rotation of 120°. Finally, a torque monitor point was created for later export of the torque at the middle bucket.

The governing equations, considering the incompressible flow and the neglect of a thermal analysis are reduced to the Eq. (1) and Eq. (2), that represent the continuity and momentum equations, respectively.

$$\nabla \cdot V = 0 \tag{1}$$

$$\rho \frac{DV}{Dt} = \rho g + \mu \nabla^2 V - \nabla p \tag{2}$$

where, ∇ is the gradient vector; V is the water speed, in m/s; ρ is the water density of 997 kg/m³; DV/Dt is the material derivative; g is the gravity acceleration of 9.81 m/s²; μ is the Newtonian dynamic viscosity, in Pa·s and p is the pressure, in N/m².

The turbulence models are characterized by additional equations. These equations are intended to be complements to assist in solving governing equations, previously described by Navier-Stokes equations, in Eq. (1) and Eq. (2).

The k-ε turbulence model has a lower computational cost, however, it is not able to capture high-shear regions in complex geometries. In contrast, the k-ω model, despite demanding a higher computational cost, is indicated to capture regions with high-shear in complex geometries.

The turbulence model chosen was the Shear Stress Transport (SST) model, this is a hybrid model that alternates between the k-ε and k-ω models, attributing a better agreement in relation to the computational costs and the results accuracy.

2.3 Boundary conditions

The construction of both domains separately allows the construction of different types of computational mesh for each one, for stationary domain, a hexahedral mesh was created, while for the rotating domain a tetrahedral mesh was created.

The inlet boundary condition was the water speed, which can be easily found by Eq. (3), considering the nozzle loss coefficient provided by the manufacturer of 0.97. The jet diameter was obtained by the continuity equation, provided by Eq (4).

$$V = 0.97\sqrt{2gH} \tag{3}$$

$$Q = V\frac{\pi d^2}{4} \tag{4}$$

where, V is the water jet speed, in m/s; g is the gravity acceleration of 9.81 m/s²; H is the head, in m; Q is the flow rate, in m³/s and d is the jet diameter, in m.

3 RESULTS AND DISCUSSION

3.1 Experimental data and mesh dependency test

The experimental data for five different operational points are contained in Tab. 1. The turbine has a brake dynamometer that allows adjustment at different speeds.

Table 1. Experimental results for different operational points. Average torque of 3 values.

Runner speed (rpm)	Torque (Nm)	Head (m)	Flow Rate (m³/s)
1200	0.3833 ± 0.0254	6.34	0.00283
1000	0.8600 ± 0.0007	6.34	0.00283
800	1.2333 ± 0.0158	6.34	0.00283
600	1.5900 ± 0.0014	6.34	0.00283
400	1.8667 ± 0.0054	6.34	0.00283

(1) measured at 25°C

The lower the rotating speed, the longer the simulations were, due to this fact, performing the mesh dependency test in these operational conditions would require more time. On the other hand, despite the higher rotating speeds having lower computational costs, the flow is not completely developed at the buckets.

The mesh dependency test is necessary to check the simulations reliability. In the Fig. 4, the mesh dependency test for the bucket at 800 rpm was performed, which represents the intermediate value of the analyzed rotating speeds.

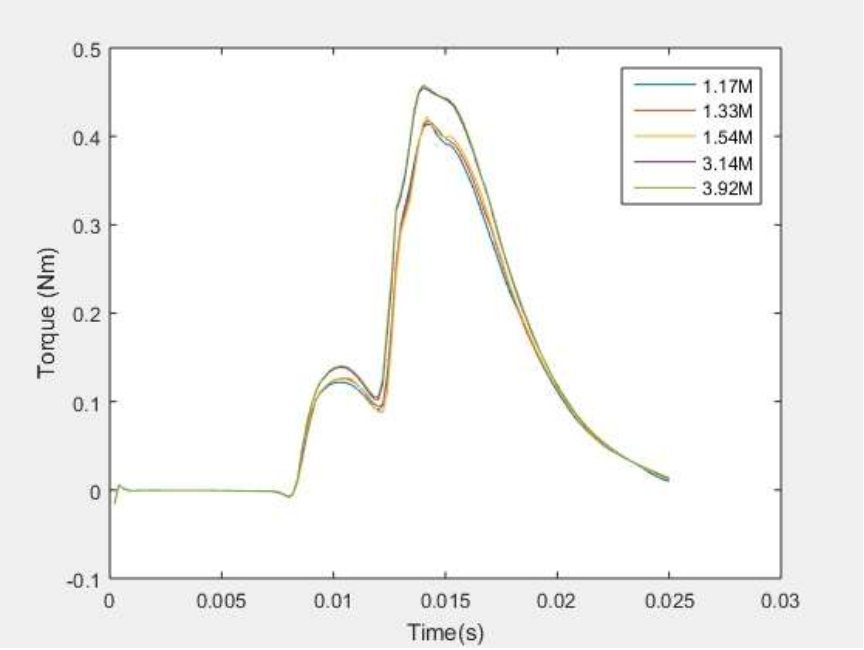

Figure 4: Mesh dependency test.

The graphic above shows five different curves of the torque generated by a single bucket over simulation time, each one with a mesh refinement. The dependency of the mesh occurred at 3.14 million cells. The chart start with a small inertial torque, followed by two peaks of torque. The first peak is related to the torque generated by the first bucket at the rear of the middle bucket and Coanda effects, while the second corresponds to the torque produced by the middle bucket through the moment differences caused by the output angle.

3.2 Total Torque

With the torque produced by the middle bucket and assuming that every bucket will come by for the same loading. It was possible, taking into account the runner frequency, to reproduce the total torque in a post-processing. The blue curve in Fig. 5 represents the total torque of the runner, corresponding to the sum of the torque contributions due to replications for a single bucket, while the red curves represent the torque of a single bucket replicated over the time. The replication of the total torque was performed using MATLAB.

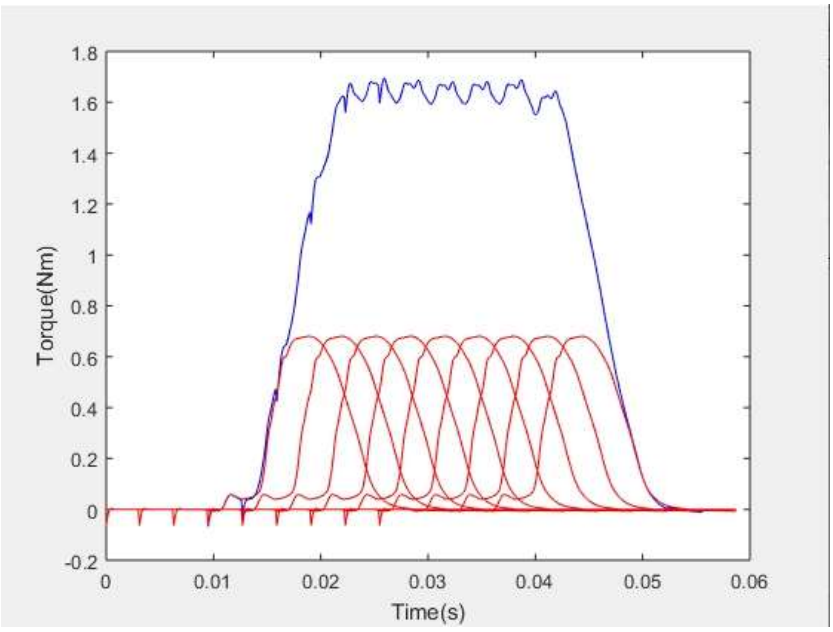

Figure 5. Total Torque for the runner speed at 600 rpm.

A stable reading of the total torque can be extracted from Time 0.0292s to 0.0324s.

The same procedure was carried out for the other operational points. Figure 6 shows the results obtained for the total runner torque, with values extracted from stable intervals as described above, and experimental torque, for all operational conditions.

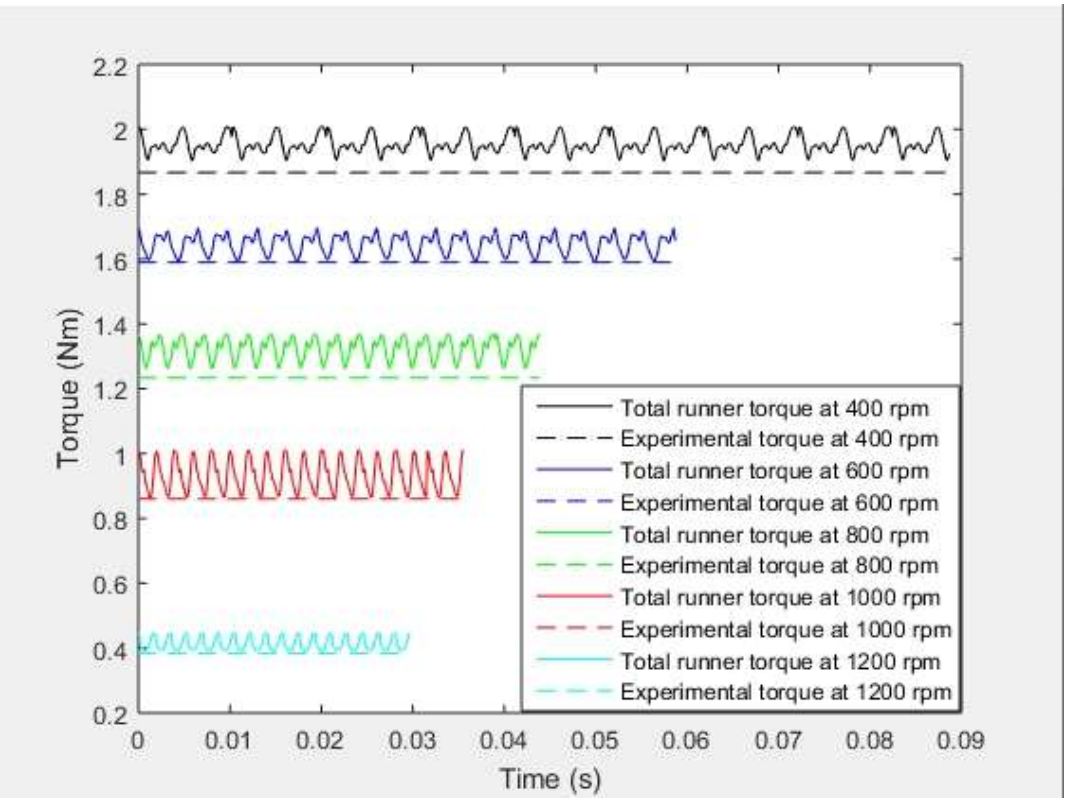

Figure 6. Total runner torque and experimental torque for all operational conditions.

Table 2 presents the general results, comparing the mean runner torque values with the experimental torque data, for all rotation speeds.

Table 2. Comparison between numerical and experimental outcomes.

Runner speed (rpm)	Experimental torque (Nm)	Mean CFD torque (Nm)	Error (%)
1200	0.3833	0.4139	7.98
1000	0.8600	0.9333	8.52
800	1.2333	1.3227	7.25
600	1.5900	1.6467	3.57
400	1.8667	1.9551	4.74

3.3 Flow visualization

Some images of the flow are shown below. In Fig. 7 and 8, at the moment of the jet cut performed by the middle bucket, it is possible to visualize the Coanda effects, which is the tendency of a fluid to take the shape of a curved surface. This fact contributes to the first peak of torque shown in Fig. 4.

The maximum torque produced by a single bucket occurs when it is more filled by the water sheet and there is the greatest fluid flow output following the path of the output angle. Figures 9 and 10 show the moment of the maximum torque produced by the middle bucket.

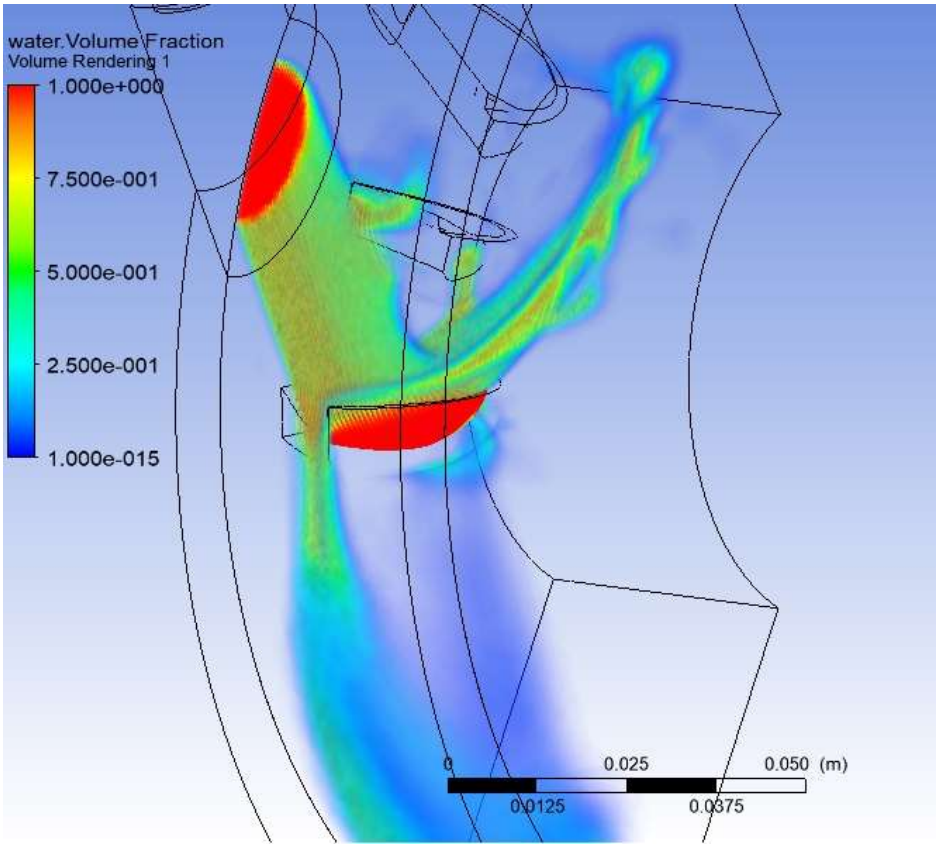

Figure 7. Coanda effects by Volume rendering for runner speed at 400 rpm.

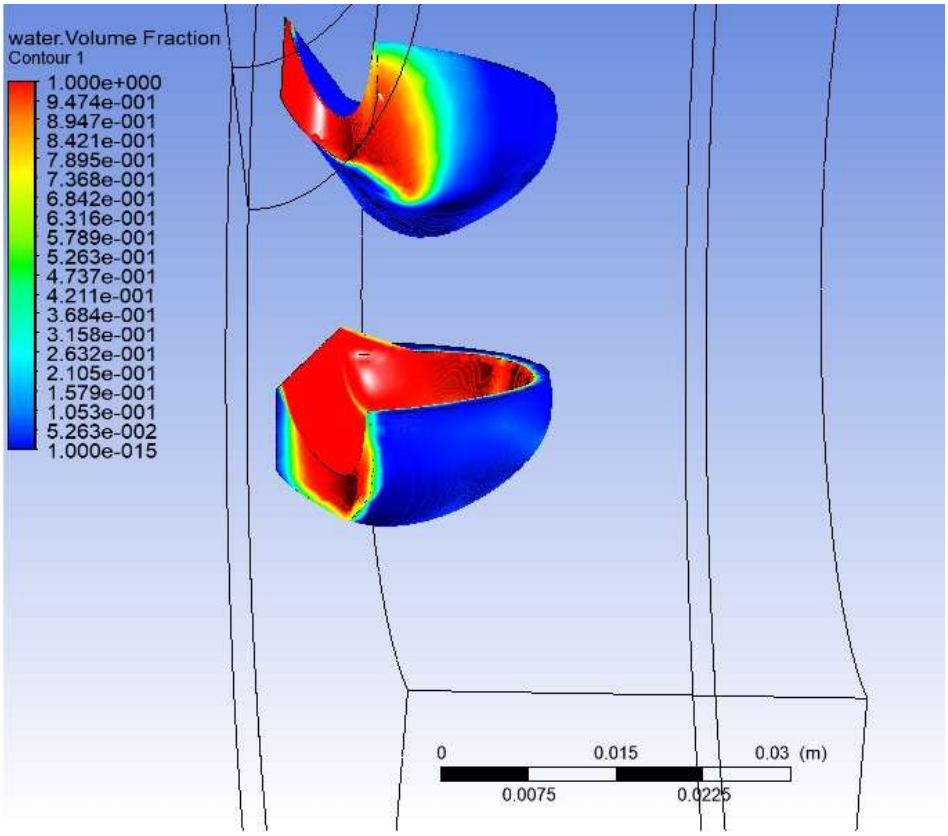

Figure 8. Coanda effects by Contour at buckets for runner speed at 400 rpm.

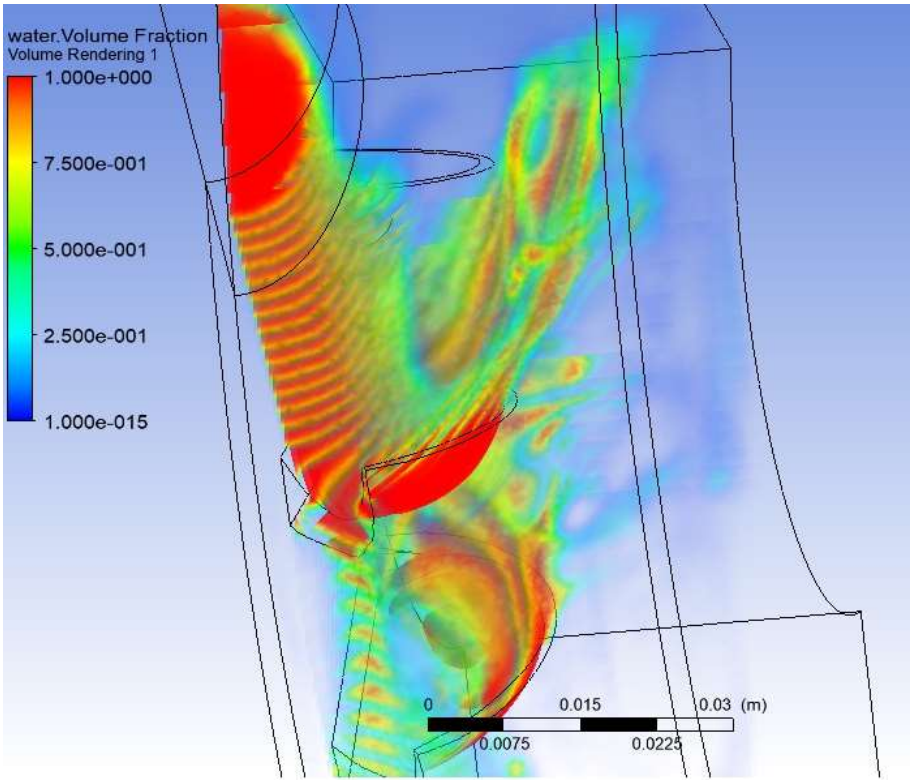

Figure 9. Maximum torque of a single bucket by Volume rendering for runner speed at 400 rpm.

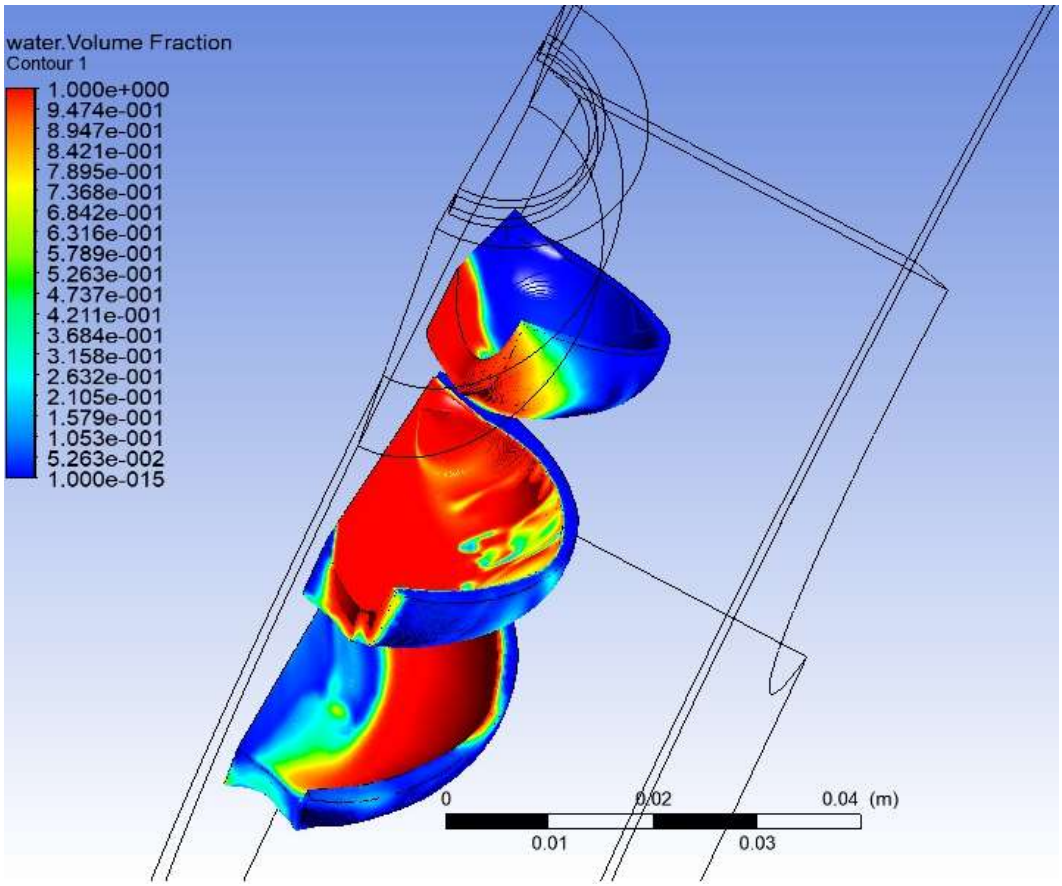

Figure 10. Maximum torque of a single bucket by Contour at buckets for runner speed at 400 rpm.

4. CONCLUSION

It is possible to state that the simulation showed excellent convergence, not only from the physical point of view, but also from the point of view of the mass balance, which was less than 1% for all simulations. A residual target of 10^{-4}, suggested by (Ansys CFX Modeling, 2017) for conservation equations, makes the simulation to take longer and, in most simulations, this target has not been reached. The values obtained for the torque by the numerical simulations overestimate the experimental values up to 8.52% and, although the nozzle losses have been accounted, this work does not include manifold and friction losses. In other words, the torque generated by the runner does not correspond to the shaft torque, measured experimentally. It is possible to conclude that the CFD model, as well as the entire geometric design, was validated to the detriment of the proximity of the experimental results with results by CFD.

5. ACKNOWLEDGEMENTS

The authors acknowledge the support from the Center of Excellence in Energy and Propulsion Systems, Laboratory of Thermal and Hydraulic Sciences, Department of Mechanical and Industrial Engineering and the Federal University of Juiz de Fora.

6. REFERENCES

ANSYS. *CFX Modeling/ Theory Guide* 17.0, 2017.

Barstad, L. F., 2012. *CFD Analysis of a Pelton Turbine*. Master's Thesis, Norwegian University of Science and Technology, Norwegian, June, p. 108, 2012.

Eisenring, M., 1991. *Micro Pelton Turbines*, GTVGATE publishing, Niederuzwill, Switzerland.

Gupta, V., Prasad, V., Khare, R., 2016. "Numerical simulation of six jet Pelton turbine model". *Energy*, v. 104, p. 24–32, 2016.

Nigussie, T., Engeda, A., Dribsa, E., 2017. "Design, Modeling, and CFD Analysis of a Micro Hydro Pelton Turbine Runner: For the Case of Selected Site in Ethiopia". *International Journal of Rotating Machinery*, v. 2017, 2017.

Panthee, A., Prasad, N. H., Thapa, B., 2014. "CFD Analysis of Pelton Runner". *International Journal of Scientific and Research Publications*, v. 4, n. 8, p. 4–9, 2014.

Rygg, J. R., 2013. *CFD Analysis of a Pelton Turbine in OpenFOAM*. Master's Thesis, Norwegian University of Science and Technology, Norwegian, June, p. 119, 2013.

Thake, J., 2000. *The Micro-Hydro Pelton Turbine Manual: Design, Manufacture and Installation for Small-Scale hydro-Power*, ITDG publishing, London , United Kingdom.

White, F. M., 2011. *Fluid Mechanics*. McGraw- Hill Higher Education, New York NY, 7rd edition.

Židonis, A. and Aggidis, G. A., 2015. "State of the art in numerical modelling of Pelton turbines". *Renewable and Sustainable Energy Reviews*, v. 45, p. 135–144, 2015.

7. RESPONSIBILITY NOTICE

The authors are solely responsible for the printed material included in this paper.